

Hemodynamic Modelling of a Stenosed Internal Carotid Artery with Newtonian and Non-Newtonian Blood Rheology

Zyad Hamed Abdelrahman Emad Yomna Sabry Sulaiman Alfozan Hamdy Ahmed
Team 4

A. Physiological and Rheological Inputs

Artery Selection and Physiological Parameters

We model the extracranial internal carotid artery (ICA), since most clinically relevant carotid stenoses are located at the origin of the ICA and are an important cause of ischaemic stroke and transient ischaemic attacks [1, 2]. The ICA is therefore a natural target for studying how stenosis modifies blood flow and wall shear stress. We initially considered the common carotid artery (CCA), but a suitable CCA geometry and design was not available within the given mesh limits, whereas an ICA template was. Because the CCA and ICA are contiguous large arteries with similar calibre and flow conditions, switching from CCA to ICA keeps the hemodynamic problem essentially the same.

In this task, we take the geometric data from the ultrasound study of Krejza *et al.* [3], who reported mean ICA diameters of **4.66 ± 0.78 mm** in women and **5.11 ± 0.87 mm** in men. In our model we use the **male ICA diameter of 5.11 mm** as the reference lumen size. We choose the male value because men have a higher burden of atherosclerosis: in a coronary CT study of 916 patients, Qureshi *et al.* found obstructive stenosis in **21%** of men vs. **11%** of women and plaque prevalence of **67.9%** vs. **51.6%**, with an adjusted odds ratio of **2.96** for men [4]. Although this study concerns the coronary arteries, it supports using the male ICA diameter as representative of a higher-risk group for stenosis, which is what we adopted in our simulation.

For the inflow we assume steady conditions with a mean inlet velocity of **0.35 m/s**, which lies inside the range of time-averaged ICA velocities ($\approx 0.3\text{--}0.4 \text{ m/s}$) reported by Doppler ultrasound and phase-contrast MRI in healthy adults [5, 6]. The blood density is set to **1060 kg/m³**, a standard value in large-artery CFD and consistent with previous carotid simulations [7, 8]. Together, these literature-based choices define a straight ICA segment with realistic diameter and flow conditions.

Blood Rheology and Parameter Values

Blood is a suspension of red blood cells in plasma and behaves as a shear-thinning fluid: its apparent viscosity is higher at low shear rates and decreases towards a lower plateau at high shear. To study how the rheological assumption influences the results, we simulate blood flow using two viscosity models: a Newtonian model with constant viscosity and a non-Newtonian Carreau–Yasuda model.

In the **Newtonian reference case**, blood is treated as an incompressible fluid with constant dynamic viscosity

$\mu_N = 3.5 \times 10^{-3} \text{ Pa}\cdot\text{s}$ and density $\rho = 1060 \text{ kg/m}^3$. This effective viscosity is commonly used for large arteries and matches the Newtonian comparison in several carotid CFD studies [7, 8].

For the **non-Newtonian case** we use the **Carreau–Yasuda** model with parameter values taken directly from the carotid simulation of Gharabi *et al.* [7]. The viscosity $\mu(\dot{\gamma})$ depends on the shear rate $\dot{\gamma}$ and smoothly transitions from a zero-shear viscosity μ_0 to an infinite-shear viscosity μ_∞ :

$$\mu(\dot{\gamma}) = \mu_\infty + (\mu_0 - \mu_\infty) [1 + (\lambda\dot{\gamma})^a]^{\frac{n-1}{a}}.$$

The parameters are $\mu_0 = 0.022 \text{ Pa}\cdot\text{s}$, $\mu_\infty = 0.002 \text{ Pa}\cdot\text{s}$, $\lambda = 0.11 \text{ s}$, $n = 0.392$ and $a = 2$, exactly as listed in their Table 1. The same parameter set has been reused in several independent CFD and FSI studies of carotid and stenosed arteries [8–10], so it can be regarded as a standard choice for large-artery blood flow; this is why we used it in our simulation.

We prefer the **Carreau–Yasuda** law over a simple **power-law** model because it behaves realistically over the full shear-rate range in stenosed arteries. Power-law models can approximate intermediate shear rates but may give unphysical viscosities at very low or very high shear and do not recover a finite Newtonian plateau. By contrast, the Carreau–Yasuda model reproduces the high- and low-shear limits of whole-blood viscosity more accurately [9]. Using both rheology models with the same geometry and boundary conditions allows us to isolate the influence of the viscosity law in the later analysis.

B. Geometric Analysis

To examine how geometry alone influences hemodynamics, we keep physiological inputs fixed and vary only the degree of stenosis in the ICA model (0%, 50% and 75% area reduction). For each Newtonian case, we compute the pressure drop ΔP as the difference in area-averaged total pressure between an inlet cross-section upstream of the stenosis and an outlet cross-section downstream of the disturbed region.

Figure 1 shows that the relationship between ΔP and the severity of the stenosis is strongly non-linear. The pressure drop increases only modestly when stenosis increases from 0% to 50%, but becomes several times larger when stenosis increases from 50% to 75%. This behavior agrees with the classical experiments of Young and Tsai on model arterial stenoses, where the pressure drop across the stenosis can be written as a sum of a linear and a quadratic term in flow rate and becomes very large once only a small residual lumen area remains [11–13].

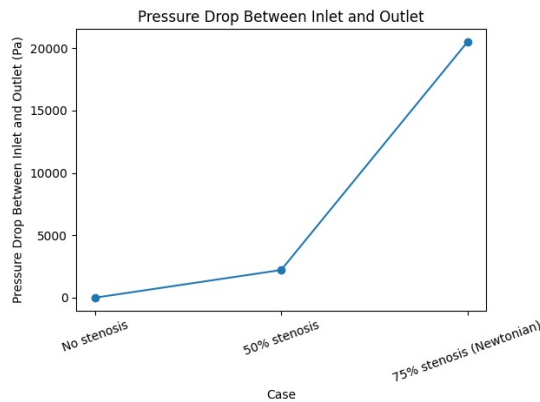


Figure 1: Pressure drop between inlet and outlet versus stenosis severity for the Newtonian simulations (Young’s curve).

More recent reduced-order models derive similar expressions directly from the Navier–Stokes equations and introduce an additional turbulence term for severe stenoses in the pressure equation [13]. Modern CFD (Computational Fluid Dynamics) studies of stenosed carotid arteries likewise report a steep, non-linear increase in pressure drop and wall shear stress as stenosis advances from moderate to severe levels [14].

From a bio-implication perspective, this non-linearity means that mild and moderate stenoses cause only small pressure losses, so flow and perfusion remain nearly normal and therefore produce few or no symptoms initially. Once stenosis enters a critical range (typically above 70% diameter reduction), however, a relatively small additional narrowing can cause a large decrease in perfusion pressure and may cause an acute ischaemic event such as stroke. Theoretical analyses of critical arterial stenosis show that beyond such thresholds, organ perfusion can collapse rapidly even though the preceding changes in symptoms were mild [15]. This helps explain why sudden cardiovascular events such as stroke or myocardial infarction are difficult to predict based only on early, mild symptoms: the underlying pressure–flow relationship is highly non-linear, and the hemodynamic impact of stenosis accelerates sharply once a critical severity is reached.

C. Rheological Comparison

Velocity Streamlines

Figure 2 compares the velocity streamlines for the 75% stenosis using Newtonian and Carreau–Yasuda rheology. In both cases a narrow high-velocity jet forms at the stenosis throat and is followed downstream by flow separation and a disturbed-flow region. With the non-Newtonian model, the shear-thinning viscosity is lower inside the high-shear jet and higher in the low-shear region, reflecting the inverse relationship between shear rate and effective viscosity, so the jet appears slightly more focused. The Newtonian model produces a more diffuse jet that spreads its influence further into the lumen [9].

Recirculation Zone

The zoomed views in Fig. 3 focus on the **post-stenotic recirculation zone**. Immediately downstream of the stenosis throat, the jet separates from the wall and forms a vortex region where some streamlines reverse direction before the flow re-attaches further downstream.

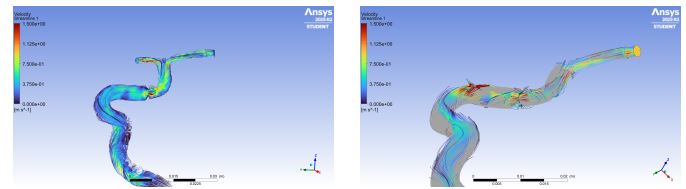


Figure 2: Velocity streamlines for the 75% stenosis case with (left) non-Newtonian Carreau–Yasuda rheology and (right) Newtonian rheology.

A vortex region is a localized area of swirling, circular blood flow that forms downstream of a stenosis due to flow separation and instability. In the non-Newtonian simulation this recirculation bubble is **slightly shorter and more damped**, which is consistent with the higher effective viscosity of shear-thinning blood in low-shear regions. In contrast, the Newtonian assumption, with its constant viscosity, **allows the separated flow to persist over a longer distance**, so the disturbed-flow region extends further downstream. Thus, in line with the question posed in the task statement (“Does the non-Newtonian viscosity make this zone longer or shorter?”), our results indicate that the non-Newtonian rheology makes the recirculation zone **shorter**, because the higher viscosity in the low-shear region more strongly damps the swirling motion and promotes earlier re-attachment of the flow.

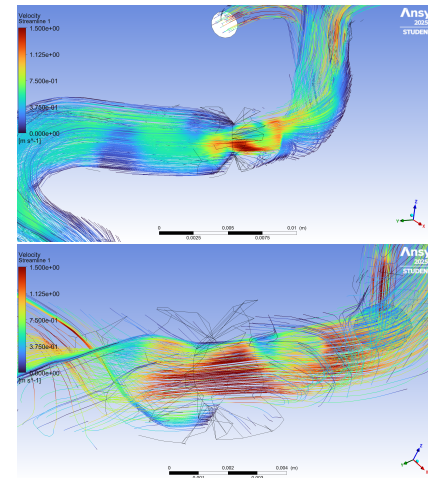


Figure 3: Zoom on the post-stenotic recirculation zone for the 75% stenosis case with (left) non-Newtonian and (right) Newtonian rheology.

Wall Shear Stress (WSS) and Bio-Implications

Figure 4 compares the wall shear stress (WSS) for the 75% stenosis case using non-Newtonian (Carreau–Yasuda) and Newtonian rheology. In both simulations the highest WSS values occur at the **stenosis throat**, where the lumen is most narrowed and the velocity jet impinges on the wall. However, the Newtonian model produces much higher peak WSS and a sharper gradient at the throat, because the viscosity is fixed and cannot decrease in the high-shear region. With the shear-thinning Carreau–Yasuda model, the effective viscosity drops at high shear rates, so the same volumetric flow can be carried with a slightly lower wall shear stress. Qualitatively, this means that a purely Newtonian assumption tends to **overestimate the peak WSS** compared with a more realistic non-Newtonian rheology.

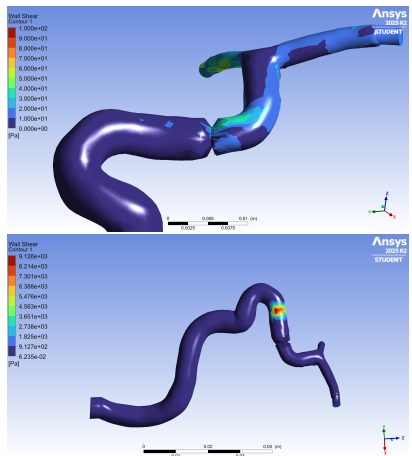


Figure 4: Wall shear stress distribution for the 75% stenosis case with (left) non-Newtonian Carreau–Yasuda rheology and (right) Newtonian rheology. Colours show WSS magnitude on the vessel wall.

Downstream of the stenosis, both rheology models exhibit an extended region of relatively low WSS on the inner wall of the recirculation zone, where the near-wall velocity is small and the flow may even reverse. This previously described vortex region coincides with low WSS on the wall, because the swirling separated flow reduces the local tangential velocity at the boundary. Numerous experimental and clinical studies have shown that such chronically low-WSS regions are strongly associated with the initiation and progression of atherosclerotic plaques [16,17]. In contrast, very high WSS at the stenosis throat is linked to plaque vulnerability and possible rupture.

Biologically, this means that the post-stenotic low-WSS zones in our simulations are plausible sites for further plaque growth and remodelling, whereas the extremely high WSS at the throat—especially in the Newtonian model—may contribute to endothelial damage and plaque destabilisation. Thus, both the magnitude and the spatial distribution of WSS are important when assessing the long-term risk of disease progression in stenosed carotid arteries.

Modelling Assumptions and Limitations

In this task we used steady, incompressible flow in a rigid-walled ICA model with a single branch. Blood was modelled either as a Newtonian fluid with constant viscosity or with the Carreau–Yasuda law, using parameter values taken from the literature. For the 75% stenosis, the flow was solved with the standard ANSYS k-epsilon turbulence model.

To decide whether turbulence should be included, we estimated the Reynolds number for the 0% stenosis case (Model 1). Using the reference diameter and mean inlet velocity, we obtained $Re \approx 541$, which lies in the laminar regime. For the stenosed geometries (50% and 75%), however, the local velocity and effective diameter vary strongly along the throat, so a single representative Reynolds number is difficult to define. We therefore assumed that the 50% stenosis case could also be modeled using a laminar solver and that the 75% stenosis case would show transitional or turbulent behavior and modeled it with the turbulence solver.

These simplifications ignore pulsatile inflow, wall motion, patient-specific geometry and the detailed transition

to turbulence. Therefore, the pressure drops and WSS patterns in our results should be viewed as qualitative trends rather than exact predictions for an individual patient. Even with these limitations, the simulations clearly show that pressure loss grows non-linearly with stenosis severity and that the choice of rheology (Newtonian vs. non-Newtonian) changes the predicted WSS and flow patterns.

Conclusion

Using an idealised internal carotid artery model, this study showed that the pressure drop across a stenosis increases in a strongly non-linear manner as the degree of narrowing becomes severe. The Young-type curve obtained from the Newtonian simulations demonstrates that increasing stenosis from 50% to 75% leads to a disproportionate rise in trans-stenotic pressure loss, explaining why critical stenoses can cause sudden deterioration in perfusion despite mild earlier symptoms.

Comparison between Newtonian and Carreau–Yasuda rheology at 75% stenosis revealed that the non-Newtonian model produces a more focused jet, a slightly shorter post-stenotic recirculation zone, and lower peak wall shear stress at the stenosis throat. The Newtonian assumption therefore tends to overestimate extreme WSS values, although both models predict similar low-WSS regions downstream that are relevant for plaque growth.

These results also highlight why simplified analytical approaches, such as Bernoulli-based formulations, are insufficient for stenosed arteries, as they neglect viscous, geometric, and turbulence-related losses that dominate once the lumen becomes critically narrowed. The classical naiver stokes equation only works for Newtonian fluids. The modified versions to account for non-Newtonian models, like Carreau–Yasuda, do not have an analytical solution. Therefore, usage of numerical computation software like ANSYS is essential. Although the model uses steady flow, rigid walls, and simplified geometry, the simulations capture clear qualitative trends, emphasizing that both stenosis severity and blood rheology play a key role in determining pressure loss, flow patterns, and wall shear stress in carotid artery disease.

References

- [1] A. Ismail, M. K. Zafar, S. Sattar, *et al.*, “Carotid artery stenosis: A look into the diagnostic and management strategies,” *Cureus*, vol. 15, no. 5, e38342, 2023.
- [2] E. Qaja and M. S. Klooster, “Symptomatic carotid artery stenosis,” in *StatPearls*. Treasure Island, FL: StatPearls Publishing, 2024.
- [3] J. Krejza, K. Szczygiel, J. Masel, *et al.*, “Carotid artery diameter in men and women and the relation to body and neck size,” *Stroke*, vol. 37, no. 4, pp. 1103–1105, 2006.
- [4] W. Qureshi, R. S. Zafar, S. Sattar, *et al.*, “Gender differences in coronary plaque composition and stenosis severity in symptomatic patients with coronary artery disease,” *Int. J. Cardiovasc. Imaging*, vol. 29, no. 8, pp. 1903–1912, 2013.
- [5] S. O. Oktar, H. Yücel, N. Ozdemir, *et al.*, “Blood-flow volume quantification in internal carotid and vertebral arteries: Comparison of 3 different ultrasound techniques with phase-contrast MR imaging,” *AJNR Am. J. Neuroradiol.*, vol. 27, no. 2, pp. 363–369, 2006.

- [6] A. Harloff, J. N. Frydrychowicz, J. Bock, *et al.*, “In vivo flow and wall shear stress assessment in the carotid artery: Comparison of 4D flow MR imaging with ultrasound,” *J. Magn. Reson. Imaging*, vol. 37, no. 2, pp. 480–489, 2013.
- [7] H. Gharahi, B. A. Zambrano, D. C. Zhu, J. K. DeMarco, and S. Baek, “Computational fluid dynamic simulation of human carotid artery bifurcation based on anatomy and volumetric blood flow rate measured with magnetic resonance imaging,” *Int. J. Adv. Eng. Sci. Appl. Math.*, vol. 8, no. 1, pp. 90–103, 2016.
- [8] D. Lopes, J. P. Santos, and R. P. Lemos, “Blood flow simulations in patient-specific geometries of the carotid artery: A systematic review,” *J. Biomech.*, vol. 99, 109578, 2020.
- [9] M. Perktold and G. Rappitsch, “Computational fluid dynamic study on effect of Carreau–Yasuda rheology in large arteries,” *J. Biomech. Eng.*, vol. 134, no. 11, 2012.
- [10] M. T. Ngo, C. I. Kim, J. Jung, *et al.*, “Four-dimensional flow magnetic resonance imaging for assessment of velocity magnitudes and flow patterns in the human carotid artery bifurcation: Comparison with computational fluid dynamics,” *Diagnostics*, vol. 9, no. 4, 223, 2019.
- [11] D. F. Young and F. Y. Tsai, “Flow characteristics in models of arterial stenoses. I. Steady flow,” *J. Biomech.*, vol. 6, no. 4, pp. 395–410, 1973.
- [12] D. F. Young and F. Y. Tsai, “Flow characteristics in models of arterial stenoses. II. Unsteady flow,” *J. Biomech.*, vol. 6, no. 5, pp. 547–559, 1973.
- [13] K. G. Lyras and J. Lee, “An improved reduced-order model for pressure drop across arterial stenoses,” *PLOS ONE*, vol. 16, no. 10, e0258047, 2021.
- [14] L. Onyami, R. M. Nalule, F. K. Mbabazi, and A. K. Muhamza, “CFD analysis of pressure and velocity profiles in stenosed carotid arteries at varying degrees of occlusion,” *Open J. Fluid Dyn.*, vol. 15, pp. 207–221, 2025.
- [15] J. P. Archie Jr., “Critical arterial stenosis revisited,” *medRxiv*, preprint, 2022, doi:10.1101/2022.04.24.22274211.
- [16] A. M. Malek, S. L. Alper, and S. Izumo, “Hemodynamic shear stress and its role in atherosclerosis,” *JAMA*, vol. 282, no. 21, pp. 2035–2042, 1999.
- [17] F. Rikhtegar, J. Bochud, N. Balabani, *et al.*, “Choosing the optimal wall shear parameter for the prediction of plaque location in human coronary arteries,” *J. Biomech.*, vol. 45, no. 15, pp. 2618–2624, 2012.